Available online at www.sciencedirect.com
SCIENCE DIRECT®
ELSEVIER
Earth and Planetary Science Letters 214 (2003) 655–668
EPSL
www.elsevier.com/locate/epsl

Silicon self-diffusion in single-crystal natural quartz and feldspar

D.J. Cherniak *

Department of Earth and Environmental Sciences, Rensselaer Polytechnic Institute, Science Center 1C25, 110 8th St., Troy, NY 12180, USA

Received 3 March 2003; received in revised form 30 June 2003; accepted 15 July 2003

Abstract

Silicon diffusion was measured in natural quartz and anorthitic feldspar under dry, low-pressure (0.1 MPa) conditions using a ^{30}Si tracer. Sources of diffusant consisted of ^{30}Si-enriched silica powder for experiments on quartz and microcrystalline ^{30}Si-doped synthetic feldspar of composition comparable to the feldspar specimens. Distributions of ^{30}Si were measured with Rutherford backscattering spectrometry and nuclear reaction analysis, using the reaction ^{30}Si (p,γ)^{31}P. The following Arrhenius relations were obtained for anneals at 1 atm in air. For quartz: transport normal to c: $D_{qtz,\perp c} = 7.97\times10^{-6}$ exp (-447 ± 31 kJ mol^{-1}/RT) m^2 s^{-1}; transport parallel to c: $D_{qtz,\parallel c} = 6.40\times10^{-6}$ exp (-443 ± 22 kJ mol^{-1}/RT) m^2 s^{-1}. For anorthitic feldspar (An$_{93}$): $D_{An} = 3.79\times10^{-7}$ exp (-465 ± 50 kJ mol^{-1}/RT) m^2 s^{-1}. The few successful experiments on diffusion in plagioclase of more albitic compositions (An$_{67}$ and An$_{23}$) reveal Si diffusivities a few orders of magnitude faster than that in the anorthite. The results for these feldspars bracket the determination of CaAl–NaSi interdiffusion under dry conditions by Grove et al. [Geochim. Cosmochim. Acta 48 (1984) 2113–2121], suggesting that the rate-limiting process is indeed Si diffusion. Si diffusion in quartz under more reducing conditions (NNO) is slightly slower (by about half an order of magnitude) than diffusion in samples annealed in air. This is consistent with observations made in studies of synthetic quartz [Béjina and Jaoul, Phys. Earth Planet. Inter. 50 (1988) 240–250].

Keywords: silicon; diffusion; quartz; feldspar; Rutherford backscattering; nuclear reaction analysis

1. Introduction

Characterization of the diffusion of major element constituents of silicate minerals is important in understanding the chemical and physical properties of these materials, and in constraining high-temperature processes such as metamorphic reactions, exsolution kinetics, creep, and phase transformations. Silicon is obviously a major constituent of silicate minerals, but its slow diffusivity in most materials has limited the number of studies in which it has heretofore been investigated. Jaoul and co-workers have successfully employed the ion beam techniques nuclear reaction analysis (NRA) and Rutherford backscattering spectrometry (RBS) to measure Si diffusion in olivine [3,4],

* Tel.: +1-518-276-8827; Fax: +1-518-276-6680.
E-mail address: chernd@rpi.edu (D.J. Cherniak).

0012-821X/03/$ – see front matter © 2003 Elsevier B.V. All rights reserved.
doi:10.1016/S0012-821X(03)00394-7

synthetic quartz [2], and clinopyroxene [2]. In this study, we report on Si diffusion in plagioclase feldspars and natural quartz.

As noted, Béjina and Jaoul [2] have measured Si diffusion in quartz. However, their experiments were run on a synthetic quartz with very low water content, which also contained low concentrations of other impurities. The presence of water or other impurities, as found in most natural quartz, may affect Si diffusivities. By investigating diffusion in natural quartz, and comparing these findings to these earlier results for Si diffusion in the synthetic material, we can evaluate the influence of such compositional differences on Si diffusivities.

In feldspars, silicon diffusion is most likely a rate-limiting factor in processes such as Al–Si ordering in the alkali feldspars [5,6] and CaAl–NaSi interdiffusion in plagioclase [1]. It may also play a significant role in the process of chemical diffusion of various divalent or trivalent ions of interest in geochronologic and/or trace element studies (e.g., Sr, Pb, rare earth elements (REE)), which may require charge-compensating species (Si and Al) to facilitate exchange with alkalis or calcium (e.g., [7,8]). The determination of Si transport rates may permit a better understanding of these processes in feldspars and enable observations of chemical zoning of major and trace elements to be used to obtain more refined information about thermal histories.

Previously, Si exchange in feldspars has only been investigated indirectly through studies of lamellar homogenization in plagioclase [1,9–11] and Al–Si ordering [12–16], at atmospheric and under high-pressure conditions at various levels of hydrogen fugacity. Although such studies provide valuable information about these processes, they do not offer a direct measure of Si self-diffusion, and estimating Si diffusivities from these measurements may be complicated by the involvement of factors other than Si transport. Measuring Si diffusion independently permits a straightforward quantification of diffusion rates and provides information that can aid in sorting out and assessing the significance of factors involved in more complex processes.

2. Experimental procedure

The experiments were performed on specimens of natural quartz and feldspar. The quartz is from Arkansas, obtained from Ward's Natural Science Establishment. The feldspars used in this study were an oligoclase (An_{23}) from North Carolina (provided by Don Miller), a labradorite (An_{67}) from Lake County, Oregon, obtained from the collection at the National Museum of Natural History (NMNH # 135512-1), and an anorthite (An_{93}) present as megacrysts in mafic lava from Pacaya Volcano, provided by Don Baker. We have previously measured Sr [7,17], Pb [8], and REE [18] diffusion in all three of these feldspars, and Ba diffusion in the oligoclase and labradorite [19]. Compositional analyses of the plagioclases are presented in Cherniak and Watson [7,17]. The labradorite and anorthite both contain some Fe ($\sim$0.02 Fe per formula unit); the oligoclase has about an order of magnitude less. The labradorite and oligoclase have minor amounts of Ba (0.02 and 0.06 wt% BaO, respectively), and some potassium (0.64 and 0.15 wt% K_2O).

Quartz specimens were cut into slabs about 0.5 mm thick and polished to 0.05 μm gamma alumina. Following polishing, quartz samples were annealed overnight at 1300°C in order to anneal damage produced in cold-working, which may produce anomalous artifacts in concentration profiles (see, for example, [20]). Fourier transform infrared spectra of quartz samples from this locality taken before and after similar thermal treatment [25] indicated virtual elimination of hydrous species with the exception of hydroxyl associated with Al in the quartz [26,27]. All of these preliminary anneals were in air, to equilibrate point defects at conditions comparable to those encountered during the diffusion anneals. Labradorite and anorthite specimens were prepared in a similar way by polishing and pre-annealing; anneals were done at 1200°C. The oligoclase was cleaved and (001) cleavage faces were used in experiments, with no pre-annealing step.

The source of diffusant for experiments on quartz was ^{30}Si-enriched silica. The silica was heated for 1 h at 1300°C in a Pt crucible, then finely ground. For the feldspar, the sources were

fine crystalline powders of ^{30}Si-doped feldspar of the same major element compositions as the specimens used in experiments. The source for the Pacaya anorthite was synthesized by combining 1 part (molar) each of $CaCO_3$, Al_2O_3, SiO_2 (of normal isotopic composition), and ^{30}Si-enriched SiO_2 (96.5% ^{30}Si). This mixture was heated slowly to 1100°C to de-carbonate the $CaCO_3$, then brought up to 1570°C for 5 h to produce a glass. The glass was then crushed and returned to the furnace at 1480°C for 1–2 days to recrystallize. The resulting anorthite was then ground, and combined with a small amount of end-member albite to approximate the major element composition of the Pacaya anorthite (i.e., An_{93}). This mixture was heated at 1400°C for a few hours, then re-ground. The source for the experiments on labradorite was synthesized in a similar way, but using a 67:33 molar ratio of the ^{30}Si-enriched anorthite to albite. The source for the oligoclase experiments consisted of a mixture of synthesized ^{30}Si-enriched albite and synthesized anorthite (of normal isotopic composition). The albite was made by combining 1 part (molar) each of Na_2CO_3 and Al_2O_3, 4 parts of ^{30}Si-enriched SiO_2 (96.5% ^{30}Si), and 2 parts of SiO_2 of normal isotopic composition. The mixture was heated slowly from 500°C to 1000°C to de-carbonate, then heated to 1200°C for a few hours. The glass was then ground, combined with synthetic anorthite (prepared as above, but without ^{30}Si-enriched SiO_2) in 77:23 molar proportion of albite:anorthite, and returned to the furnace at 1200°C for a few hours. The furnace temperature was then lowered to 1125°C and the crucible containing the albite–anorthite mix was left in overnight to crystallize; it was then ground for use in the diffusion experiments. Source materials were finely ground, but no attempt was made to sieve to ensure a uniform range of grain sizes.

The prepared feldspar and quartz samples were placed in Pt capsules with their respective sources and annealed in 1 atm vertical tube furnaces for times ranging from 30 min to 2 months at temperatures from 1025 to 1450°C. Source material was packed tightly around specimens, with polished surface down in the capsule. Experiments run at 1100°C and above were done in Deltech tube furnaces with $MoSi_2$ heating elements; those below 1100°C were run in Kanthal-wound tube furnaces. Temperatures in the former case were monitored with Pt10%Rh–Pt (type S) thermocouples, with those in the latter monitored with chromel–alumel (type K) thermocouples. Temperature uncertainties in both cases were typically ±2°C. After diffusion anneals, the sample capsules were simply quenched by removing them from the furnace and permitting them to cool in air. The cooled samples were then removed from capsules and freed of residual source material clinging to surfaces by ultrasonic cleaning in baths of distilled water and ethanol. Sources of diffusant selected were readily removed from mineral surfaces. Optical examination and scanning electron microscopy imaging of surfaces following cleaning revealed only isolated grains remaining, with sufficiently large areas of the sample free from source material for useful analysis.

A few experiments were run under buffered conditions in Deltech furnaces. CO–CO_2 gas mixtures were used to maintain desired fO_2 conditions (equivalent to Ni–NiO buffer), with fO_2 monitored with a zirconia sensor. For quartz and feldspar specimens used in buffered experiments, the pre-annealing step described above was performed under buffered conditions using sealed silica glass capsules containing the sample and a solid buffer (to buffer at Ni–NiO).

3. RBS and NRA analyses

The RBS and NRA analyses were performed at the 4 MeV Dynamitron accelerator at the University at Albany-SUNY. Samples were mounted in the chamber at a 7° tilt from normal to discourage channeling, especially in the quartz. For RBS, a beam of $^4He^+$ ions was used, with backscattered ions detected by a silicon surface barrier detector. Samples were analyzed using either a 2 or 3 MeV beam. Beam spot size for analysis was typically about 1 mm^2. For each sample, a number of brief analyses were collected at several spots on the sample surface to test for reproducibility and to determine whether unusual surface conditions might exist on a region of the sample that would

produce anomalous profiles, and also to check for the occurrence of channeling. Following such reconnaissance, RBS spectra were taken with longer acquisition times (typically 45–60 min). Spectra of untreated quartz and feldspars were also taken under the same analytical conditions to facilitate evaluation of backgrounds for the RBS signal from ^{30}Si in spectra from diffusion anneals. Comparison of these spectra also provides confirmation of the expected $^{30}Si \rightarrow {}^{28}Si$ exchange occurring in self-diffusion with a ^{30}Si-enriched source. Further details of the analytical procedures and data reduction protocols employed are outlined elsewhere [7].

NRA was done using the 620 keV resonance of the $^{30}Si(p,\gamma)^{31}P$ nuclear reaction (e.g., [2,21]), using an incident proton beam. The 7.9 MeV γ-rays produced in the reaction were collected with a BGO scintillation detector. Beam energy was increased gradually, in steps of one to a few keV, to probe ^{30}Si into the sample. NRA was used only on quartz samples because of interferences in the gamma spectra of the feldspars from products of the $^{27}Al(p,\gamma)^{28}Si$ reaction.

Concentration profiles derived from the RBS spectra were fit with a model to determine the diffusion coefficient, D. In this case, the process is modeled as simple one-dimensional diffusion in a semi-infinite medium with a source maintained at constant concentration. Although the powder sources employed are not in the truest sense 'uniform' or 'continuous' distributions since contact with the sample surface is at discrete points, theoretical evaluations [22] suggest that no error is introduced into determinations of diffusion coefficients (given a linear, one-dimensional, concentration-independent model for diffusion in an isotropic medium) when the source material is distributed non-uniformly over the sample surface. Our previous experiences with such sources (e.g., [7,23]) are also consistent with this finding, and profiles do appear to correspond reasonably well to that expected for a simple complementary error function solution. Modeling was also done to test the effects of discontinuous sources of various geometries on the appearance of diffusion profiles, using analytical solutions to the diffusion equation adapted from the expressions of Carslaw and Jaeger ([24], section 10.5) for circular and rectangular sources of limited dimension with constant heat supply. A sum of profiles produced by a two-dimensional array of these sources was used to simulate the surface conditions and consequent profiles, with results compared to a curve of a complementary error function. Such simulations and comparisons yield diffusivities that agree within a factor considerably smaller than the analytical uncertainties for profiles in this work, so significant error is not introduced in assuming the profiles conform to a complementary error function solution.

Diffusivities are calculated by plotting the inverse of the error function of $[(C_o - C(x,t))/C_o]$ vs. the depth x, which yields a straight line (should the data conform to the model) of slope $(4Dt)^{-1/2}$. C_o, the surface concentration, cannot be measured precisely because of limitations in

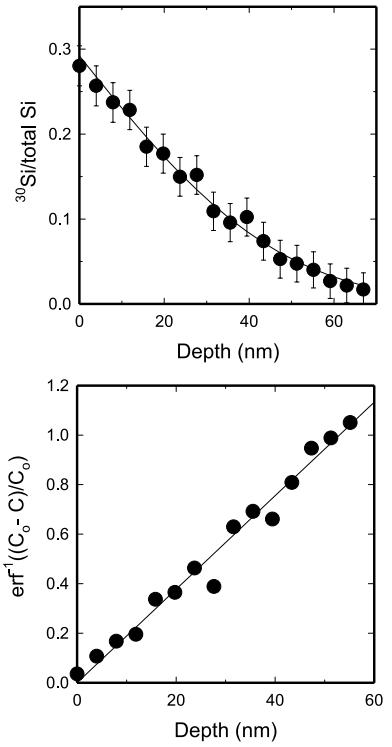

Fig. 1. Typical diffusion profiles for an Si diffusion experiment in anorthite. Profiles was measured by RBS. (a) The diffusion data are plotted with complementary error function curves. (b) The data are inverted through the error function. The slope of the line is equal to $(4Dt)^{-1/2}$.

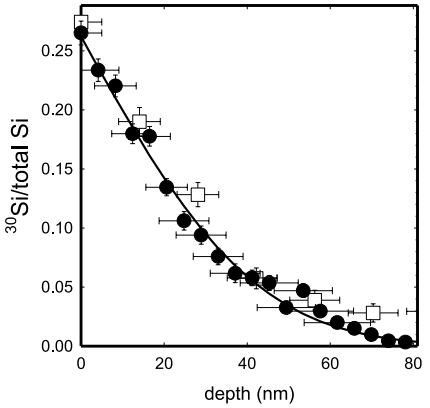

Fig. 2. Comparison of ^{30}Si diffusion profiles in quartz measured using RBS (shaded circles) and NRA with the ^{30}Si(p,γ)^{31}P reaction (white squares). Similar results are obtained with both techniques.

depth resolution of RBS, but the fitting routine provides for a determination of C_o by allowing the parameter to vary until the intercept of the line converges to zero.

Typical diffusion profiles and their inversions through the error function are shown in Fig. 1. Each of the points represents the contribution from a particular channel in the RBS spectrum. Uncertainties in diffusivities extracted from depth profiles were determined by the uncertainties in measurements of concentration and depth. The former is a function primarily of counting statistics in the RBS spectra, while the latter is determined mainly by the energy resolution of the surface barrier detector used to detect the backscattered particles and by the energy straggle of the ions as they travel in and out of the sample. In quartz, little background is present to interfere

Table 1
Si diffusion in feldspar

	Temp. (°C)	Time (s)	D (m^2 s^{-1})	log D	±	$2\sqrt{Dt}$ (m)	Buffer
Anorthite (An_{93})							
AnSi-12	1250	4.48×10^{6}	6.15×10^{-23}	−22.21	0.23	3.32×10^{-8}	air
AnSi-10	1300	1.21×10^{6}	1.28×10^{-22}	−21.89	0.24	2.49×10^{-8}	air
AnSi-6	1350	3.28×10^{5}	3.27×10^{-22}	−21.49	0.22	2.07×10^{-8}	air
AnSi-14	1392	2.59×10^{5}	5.23×10^{-22}	−21.28	0.26	2.33×10^{-8}	NNO
AnSi-7	1400	3.35×10^{5}	7.71×10^{-22}	−21.11	0.25	3.21×10^{-8}	air
AnSi-8	1400	5.26×10^{5}	1.33×10^{-21}	−20.88	0.15	5.29×10^{-8}	air
AnSi-13	1400	1.02×10^{5}	2.13×10^{-21}	−20.67	0.30	2.95×10^{-8}	air
AnSi-3	1400	1.48×10^{5}	1.00×10^{-21}	−21.00	0.22	2.43×10^{-8}	air
AnSi-4	1450	1.73×10^{5}	2.68×10^{-21}	−20.57	0.12	4.31×10^{-8}	air
AnSi-9	1450	7.20×10^{4}	3.83×10^{-21}	−20.42	0.19	3.32×10^{-8}	air
Labradorite (An_{67})							
Diffusion normal to (001)							
LabSi-7c	1055	3.11×10^{6}	1.84×10^{-22}	−21.74	0.14	4.78×10^{-8}	air
LabSi-3	1100	6.05×10^{5}	1.15×10^{-21}	−20.94	0.35	5.28×10^{-8}	air
LabSi-4c	1150	3.51×10^{5}	1.56×10^{-21}	−20.81	0.15	6.37×10^{-8}	air
LabSi-5c	1101	1.37×10^{6}	7.94×10^{-22}	−21.10	0.14	6.60×10^{-8}	air
LabSi-6c	1143	4.23×10^{5}	7.33×10^{-22}	−21.13	0.27	3.52×10^{-8}	NNO
Diffusion normal to (010)							
LabSi-7b	1055	3.11×10^{6}	1.21×10^{-22}	−21.92	0.18	3.88×10^{-8}	air
LabSi-4b	1150	3.51×10^{5}	1.44×10^{-21}	−20.84	0.19	4.50×10^{-8}	air
LabSi-5b	1101	1.37×10^{6}	7.83×10^{-22}	−21.11	0.08	6.55×10^{-8}	air
LabSi-6b	1143	4.23×10^{5}	1.32×10^{-21}	−20.88	0.18	4.73×10^{-8}	NNO
Oligoclase (An_{23})							
Diffusion normal to (001)							
OligSi-2	1080	9.32×10^{5}	2.60×10^{-22}	−21.59	0.12	3.11×10^{-8}	air
OligSi-3	1025	3.37×10^{6}	1.05×10^{-22}	−21.98	0.20	3.76×10^{-8}	air

with the ^{30}Si signal in the backscatter spectra. In the plagioclase feldspars, however, the ^{30}Si rests on the signal from α-particles backscattered from Ca in the feldspar matrix. The additional uncertainties in concentration determination that are a consequence of this interference are incorporated into procedures for data reduction. This is done by considering the uncertainty to vary as $2(N_b+N_o)^{1/2}/N_o$, where N_o is the total number of counts in the multichannel analyzer channel, and N_b is the number of counts in the background in that channel.

The primary source of uncertainty in depth in the NRA analysis is due to energy straggling, a spread in the energies of the ions comprising the incident beam as they lose varying amounts of energy (through interactions with electrons of atoms in the sample) traveling through the material. Straggling can be approximated by a Gaussian curve, with its width increasing with depth in the material as the energy spread of the ions increases as they travel greater distances.

The majority of diffusion profiles were measured with RBS, but in the few cases where NRA and RBS measurements were made on the same sample, there is good agreement (Fig. 2).

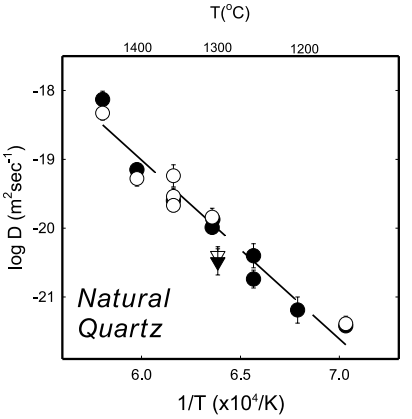

Fig. 3. Arrhenius plot for Si diffusion in natural quartz. Plotted are results for diffusion parallel (dark circles) and perpendicular (white circles) to c. The line is a least-squares fit to the diffusion data for natural quartz for transport parallel to c. Arrhenius parameters extracted from the fit are: activation energy 443 ± 22 kJ mol^{-1} and pre-exponential factor 6.40×10^{-6} m^2 s^{-1} (log $D_o = -5.19 \pm 0.76$). Little anisotropy for Si diffusion is evident, as diffusivities in quartz parallel (white circles) and perpendicular (black circles) to c are similar. The triangles are data from experiments run under buffered (NNO) conditions, with filled symbols for diffusion parallel to c and open symbols for diffusion perpendicular to c; diffusivities under these more reducing conditions are slightly slower than those for experiments run in air.

4. Results

The results from the diffusion experiments for quartz are presented in Table 1, and plotted in Fig. 3. From least-squares fits to the diffusion data on Arrhenius plots, we obtain the following diffusion parameters for the quartz: activation energy 447 ± 31 kJ mol^{-1} and pre-exponential factor 7.97×10^{-6} m^2 s^{-1} (log $D_o = -5.10 \pm 0.97$) for diffusion normal to c; and 443 ± 22 kJ mol^{-1} and pre-exponential factor 6.40×10^{-6} m^2 s^{-1} (log $D_o = -5.19 \pm 0.76$) for diffusion parallel to c. It is clear that there is little anisotropy in Si diffusion in quartz. Results for diffusion under more reducing conditions (NNO) show slightly slower diffusivities (by ~ 0.5 log unit).

The results for Si diffusion in feldspar are plotted in Fig. 4 and shown in Table 2. For anorthitic feldspar (An_{93}), an activation energy of 465 ± 50 kJ mol^{-1} and pre-exponential factor 3.79×10^{-7} m^2 s^{-1} (log $D_o = -6.42 \pm 1.57$) are found. We were unable to obtain diffusivities over a sufficiently large temperature range for either oligoclase or labradorite to establish Arrhenius parameters without large uncertainties, but a fit to the (010) data for labradorite yields an activation energy of 419 ± 99 kJ mol^{-1} and pre-exponential factor of 5.7×10^{-6} m^2 s^{-1}. There appears to be little anisotropy in Si diffusion for labradorite over the investigated temperature range. Si diffusivities for both oligoclase and labradorite are faster than those for anorthite. For both anorthite and labradorite, diffusivities under NNO-buffered conditions do not differ significantly from those obtained for experiments run in air.

A time series of diffusion anneals at 1400°C for anorthite (Fig. 5) reveals similar diffusivities for experiments differing in duration by more than a factor of five, suggesting that the dominant process being measured is indeed volume diffusion of Si.

5. Comparison with other studies

In Fig. 6, existing Si diffusion data for quartz are plotted. Giletti et al. [25] measured diffusion in natural quartz, using ^{30}Si-enriched SiO_2 deposited on the surface as a source, with depth profiling done by secondary ion mass spectrometry. They obtained diffusivities of 4.8×10^{-20} m^2 s^{-1} at 1028°C and 5.4×10^{-21} m^2 s^{-1} at 912°C, but state that diffusivities may be overestimated because of the shortness of the diffusion profiles. Béjina and Jaoul [2] measured Si diffusion in synthetic quartz by RBS and NRA; the diffusant (^{30}Si) was introduced from a RF-sputtered surface layer of ^{30}Si-enriched SiO_2. They obtained an activation energy of 746 ± 215 kJ mol^{-1} and pre-exponential factor of 2.9×10^3 m^2 s^{-1}. Although this activation energy is considerably higher than that determined in the present study, the data obtained for Si diffusion by Béjina and Jaoul [2] for diffusion experiments run in air plot on an up-temperature extrapolation of the Arrhenius line determined in the present study (Fig. 7a). The remainder of their low-pressure experiments were run under more reducing conditions (log pO_2 (in atm.) from −7.7 to −9.6); Si diffusivities for these experiments are generally slower than those for experiments run in air (Fig. 7b). These data, as well as our findings for experiments buffered at NNO, suggest that Si diffusion in quartz is somewhat slower under reducing conditions. Discrepancies between the diffusivities measured in the present study and those from [2] may also be due to the differences in amount and type of impurities present in natural vs. synthetic quartz, which may have an effect on diffusivities. Further,

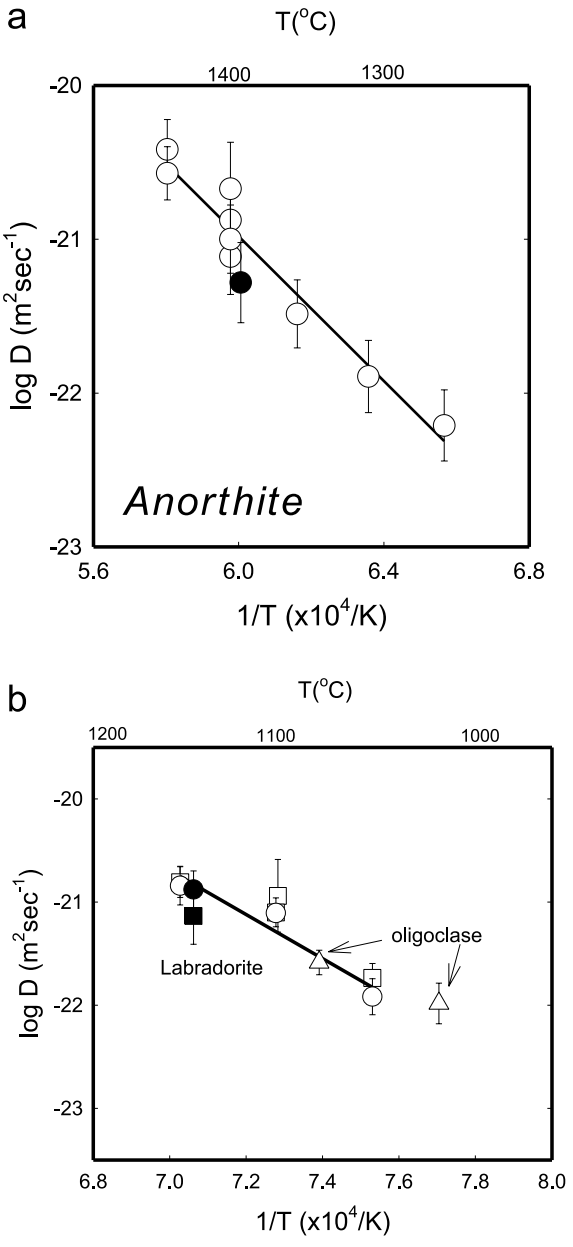

←

Fig. 4. Arrhenius plots for Si diffusion in feldspar. In panel a, diffusion in anorthite is plotted. For anorthitic feldspar (An_{93}), an activation energy of 465 ± 50 kJ mol^{-1} and pre-exponential factor 3.79×10^{-7} m^2 s^{-1} (log $D_o=-6.42\pm1.57$) are obtained. White circles are diffusivities for experiments run in air. The filled circle is for an experiment run under buffered (NNO) conditions, showing a diffusivity comparable to those obtained for the experiments run under more oxidizing conditions. In panel b data for Si diffusion in labradorite (An_{67}, squares and circles) and oligoclase (An_{23}, triangles) are shown. We were unable to obtain diffusivities over a sufficiently large temperature range for either oligoclase or labradorite to establish Arrhenius parameters without large uncertainties; a fit to the (010) data for labradorite yields an activation energy of 410 kJ mol^{-1} and pre-exponential factor of 2×10^{-6} m^2 s^{-1}. Little anisotropy for Si diffusion is evident, as diffusivities in labradorite normal to (010) (white circles) and normal to (001) (white squares) are similar, as are those for experiments buffered at NNO (black squares and circles for diffusion normal to (001) and (010), respectively).

Table 2
Si diffusion in natural quartz

	Temp. (°C)	Time (s)	D (m^2 s^{-1})	log D	±	$2\sqrt{Dt}$ (m)	Buffer
Diffusion normal to c							
QSi-12a	1149	1.95×10^{6}	3.82×10^{-22}	−21.42	0.06	5.46×10^{-8}	air
QSi-4	1200	5.22×10^{5}	6.50×10^{-22}	−21.19	0.19	3.68×10^{-8}	air
QSi-3	1250	2.30×10^{5}	1.80×10^{-21}	−20.74	0.13	4.07×10^{-8}	air
QSi-2	1250	1.69×10^{5}	3.97×10^{-21}	−20.40	0.18	5.18×10^{-8}	air
QSi-1	1299	7.56×10^{4}	1.34×10^{-20}	−19.87	0.08	6.37×10^{-8}	air
QSi-9a	1293	1.86×10^{5}	4.02×10^{-21}	−20.40	0.13	5.47×10^{-8}	NNO
QSi-5a	1300	8.64×10^{4}	1.03×10^{-20}	−19.99	0.08	5.97×10^{-8}	air
QSi-6a	1350	3.36×10^{4}	2.53×10^{-20}	−19.60	0.12	5.83×10^{-8}	air
QSi-7a	1400	9.00×10^{3}	7.00×10^{-20}	−19.15	0.08	5.02×10^{-8}	air
QSi-8a	1450	1.80×10^{3}	7.47×10^{-19}	−18.13	0.12	7.33×10^{-8}	air
Diffusion parallel to c							
QSi-12c	1149	1.95×10^{6}	4.08×10^{-22}	−21.39	0.11	5.64×10^{-8}	air
QSi-9c	1293	1.86×10^{5}	3.23×10^{-21}	−20.49	0.19	4.90×10^{-8}	NNO
QSi-5c	1300	8.64×10^{4}	1.43×10^{-20}	−19.84	0.13	7.03×10^{-8}	air
QSi-11	1350	7.20×10^{3}	5.74×10^{-20}	−19.24	0.16	4.07×10^{-8}	air
QSi-6c	1350	3.36×10^{4}	2.86×10^{-20}	−19.54	0.12	6.20×10^{-8}	air
QSi-10	1350	8.64×10^{4}	2.14×10^{-20}	−19.67	0.09	8.60×10^{-8}	air
QSi-7c	1400	9.00×10^{3}	5.19×10^{-20}	−19.28	0.11	4.32×10^{-8}	air
QSi-8c	1450	1.80×10^{3}	4.70×10^{-19}	−18.33	0.10	5.82×10^{-8}	air

the synthetic quartz used by Béjina and Jaoul [2] has a very low H_2O content (0.1 ppm H/Si), in contrast to the natural quartz. Although most of the hydrous species in the natural specimens should be eliminated through the pre-annealing treatment (e.g., [26]), hydroxyl associated with Al in natural quartz will remain (e.g., [27,28]).

No direct measurements of Si diffusion exist for feldspars other than the present study. However, rates of CaAl–NaSi interdiffusion have been determined through lamellar homogenization experiments ([1,11,12]; Fig. 8). Such interdiffusion studies may shed light on Si diffusion rates, since the process may be rate-limited by the slowest-diffusing species. Given the fact that diffusivities generally decrease with increasing charge, Si is likely the slowest-diffusing species among these elements. However, it should be noted that deter-

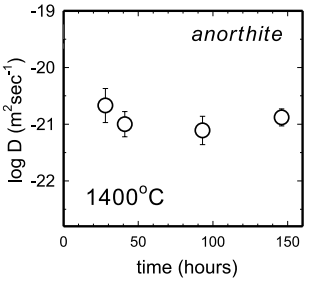

Fig. 5. Time series for Si diffusion anneals on anorthite. Diffusivities at 1400°C are generally quite similar for anneal times differing by a factor of more than five, indicating that what is being measured is volume diffusion.

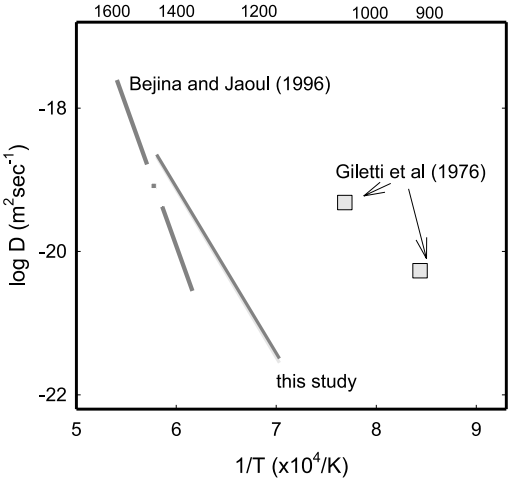

Fig. 6. Summary of measurements for Si diffusion in quartz, comparing the results from this study with measurements of Si diffusion in synthetic quartz by Béjina and Jaoul [2] and the findings of Giletti et al. [25] for natural quartz.

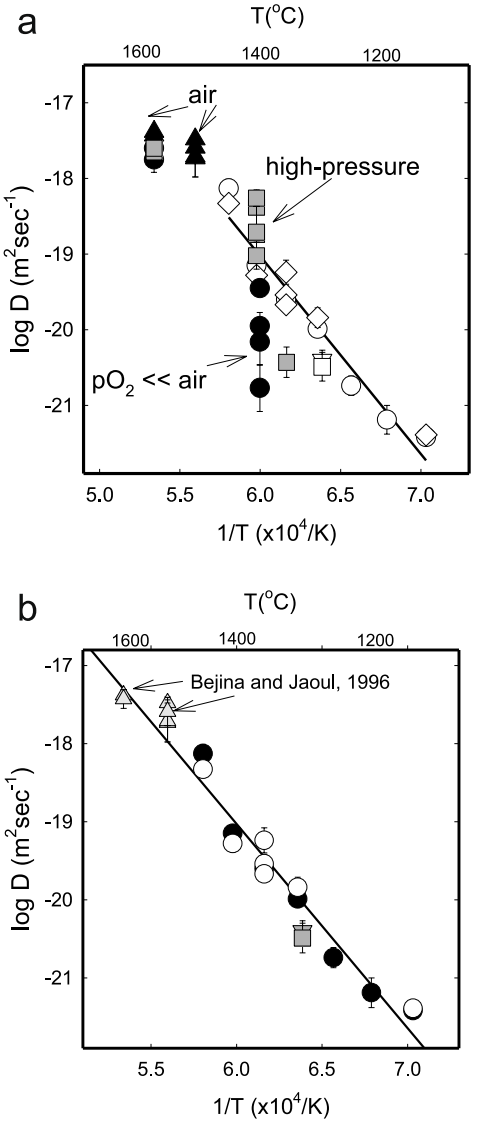

Fig. 7. Comparison of Si diffusion data for quartz from the present study (white symbols) with the data from Béjina and Jaoul [2] in synthetic quartz (shaded symbols). Panel a includes both high-pressure and low-pO_2 experiments. For results from the present study, white diamonds are for diffusion normal to c (annealed in air), white circles are for diffusion parallel to c (annealed in air) and white square and triangle are for diffusion in experiments buffered at NNO. For the data of Béjina and Jaoul, the shaded squares are for high-pressure experiments, the black circles are for experiments with $pO_2 \ll$ air, and the black triangles are for anneals in air. In panel b, only the results from [2] for diffusion in air are plotted (shaded triangles), showing that these data plot on an up-temperature extrapolation of the Arrhenius relation measured in the present work.

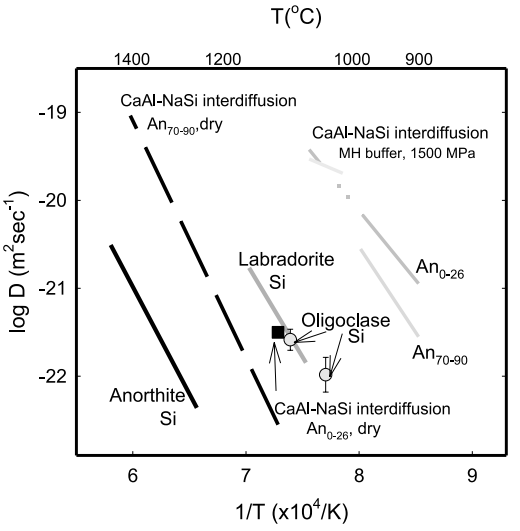

Fig. 8. Comparison of Si diffusivities in feldspar with CaAl–NaSi interdiffusion rates. Sources for data: CaAl–NaSi (An_{70-90}, dry): [1]; CaAl–NaSi (An_{0-26}, dry): [9]; CaAl–NaSi (An_{0-26}, An_{70-90}, 1500 MPa): [11]. Si diffusivities for labradorite and anorthite bracket CaAl–NaSi interdiffusion for bytownite under dry conditions, consistent with Si diffusion as the rate-limiting species in CaAl–NaSi interdiffusion.

minations of diffusivities derived from the lamellar homogenization method are limited by uncertainties in assessing homogenization times (e.g., [29]), among other factors.

In the first set of experiments, Grove et al. [1] obtained an activation energy of 516 ± 19 kJ mol^{-1} and pre-exponential factor for CaAl–NaSi interdiffusion in bytownite (An_{80}) under dry conditions over the temperature range 1100–1400°C. Yund [9] determined interdiffusion for the peristerite interval under dry conditions at 1100°C. Liu and Yund [11] have measured CaAl–NaSi interdiffusion under hydrothermal conditions (and buffered at MH) for both a bytownite (An_{70-90}) and peristerite ($\sim An_0$ to $\sim An_{26}$). For the bytownite, they obtain an activation energy of 371 kJ mol^{-1} and pre-exponential factor of 1.1×10^{-5} m^2 s^{-1} over the temperature range 900–975°C, and activation energy of 103 kJ mol^{-1} and pre-exponential factor of 4×10^{-16} m^2 s^{-1} for temperatures from 1000 to 1050°C. For the more sodic plagioclase, they obtain an activation energy of 303 kJ mol^{-1} and pre-exponential factor of

3×10^{-8} m^2 s^{-1} over the temperature range 900–1050°C. Baschek and Johannes [29] have measured NaSi–CaAl interdiffusion rates in peristerite (An_{2-18}) and obtain an activation energy of 465 kJ mol^{-1} and pre-exponential factor of 1.7×10^{1} m^2 s^{-1}.

The activation energy for CaAl–NaSi interdiffusion measured in [1] under dry conditions agrees within experimental uncertainty with the value for the activation energy for Si diffusion in anorthite measured in the present study. CaAl–NaSi interdiffusion is somewhat faster than Si diffusion in anorthite, but is slower than Si diffusion in labradorite, which is consistent with a trend of higher diffusivities for plagioclase feldspars having higher Na contents observed for diffusion of other cations. The diffusivity obtained by Yund [9] for CaAl–NaSi interdiffusion in peristerite is quite similar to values for Si diffusion in oligoclase. These findings suggest that Si diffusion is the rate-limiting factor in CaAl–NaSi interdiffusion in plagioclase, which would not be a particularly surprising conclusion.

The variation of cation diffusivities with plagioclase composition has also been noted in other work. Liu and Yund [11] observe that for NaSi–CaAl interdiffusion under hydrothermal conditions interdiffusion rates for the peristerites are higher than for bytownite. Similar trends of faster diffusivities in more sodic plagioclase are noted for other cations, including Sr [7,17,30], Pb [8], Ba [19], and the REE [18]. In Si diffusion, however, there is apparently not a systematic increase in Si diffusivities with increasing Na content across the entire plagioclase series, as has been noted for these other cations. Although data are limited, our results suggest that Si diffusivities in labradorite and oligoclase are similar. The reasons for this difference are unclear, but it may be a consequence of the different sites occupied by the respective cations and differences in diffusion mechanisms. Sr, Pb, Ba and the REE will likely occupy the Ca–Na sites in plagioclase, and given their size probably diffuse via a vacancy mechanism. In contrast, Si occupies the tetrahedral sites, and is considerably smaller in size so may diffuse via an interstitial mechanism. It is possible that Si diffusion rates are influenced by the Al:Si ratio of feldspars, and the degree of Al–Si ordering, but there is not an obvious simple relationship. It is clear that more data are necessary to better understand how these factors and others affect Si diffusion in plagioclase, and to define the mechanism for diffusion.

Liu and Yund [11] measure considerably faster (by about four orders of magnitude) CaAl–NaSi interdiffusion under hydrothermal conditions than do Grove et al. [1] under dry conditions; this has also been observed for the peristerite interval [9,10,29]. We have not yet successfully run hydrothermal experiments to investigate Si diffusion in feldspars, so can offer no comment on whether hydrothermal conditions might accelerate Si diffusion.

6. Diffusion of other species in feldspars

Cation diffusion in feldspars has been extensively studied. However, most of this work has focused on measuring diffusion of cations that substitute on sites normally occupied by the major constituents Ca, Na and K. In plagioclase, diffusion of univalent cations K and Na [31], the divalent cations Sr [7,17,30], Pb [8], Ca [32,33], Mg [32], and Ba [19], as well as trivalent REE [18] have been measured. These data are plotted in Fig. 9, along with the Si diffusion results from the present work. In all cases, Si diffusion is considerably slower than diffusion of any of the other species. This is likely due to both the high charge of Si and the comparatively large site energies for tetrahedral sites in feldspars (e.g., [34]).

In quartz, diffusion measurements of other cations have mostly explored the migration of alkalis, which likely travel interstitially through the quartz lattice. These data are plotted in Fig. 10. Pankrath and Flörke [35] have estimated Al diffusion rates from electron paramagnetic resonance measurements. Here again, Si is the slowest-diffusing species, with only Al, which presumably exchanges on the Si site, approaching within a few orders of magnitude. Also plotted is oxygen diffusion under dry conditions [36–38]. Oxygen diffusion is also faster, and has a smaller activation energy for diffusion, than silicon.

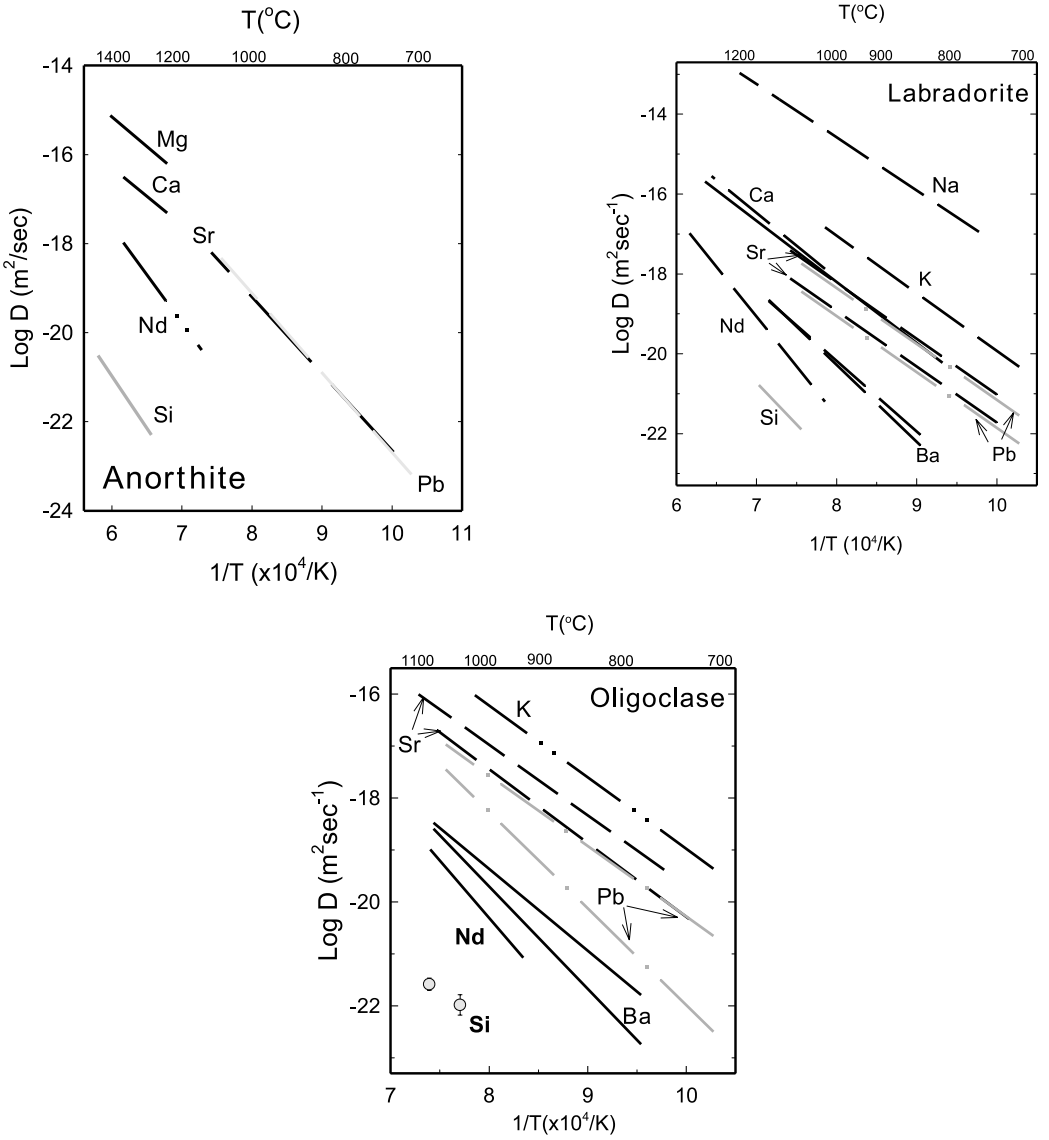

Fig. 9. Summary of cation diffusion in the three plagioclase feldspar compositions investigated in this work. Sources for data: K, Na: [31]; Ca in labradorite: [33]; Ca and Mg in anorthite: [32]; Pb: [8]; Sr: [7,17]; Ba: [19]; Nd: [18]; Si: this study.

7. Si diffusion in other minerals

Si diffusion has now been measured in a range of silicate minerals; these data are summarized in Fig. 11. Jaoul et al. [39] and Houlier et al. [4] have both proposed an interstitial mechanism for Si diffusion in synthetic quartz and iron-bearing San Carlos olivine, respectively. Béjina and Jaoul [40] found that the diffusion parameters obtained for Si diffusion in silicates conform to a linear compensation law when the activation energy for diffusion is plotted as a function of the log of the pre-exponential factor. They argue that this may be explained by the 'strain energy' model proposed in [41], in which the Gibbs free energy of diffusion is considered the 'elastic work' required to place the defect in its excited state for migration within the lattice. They note that differ-

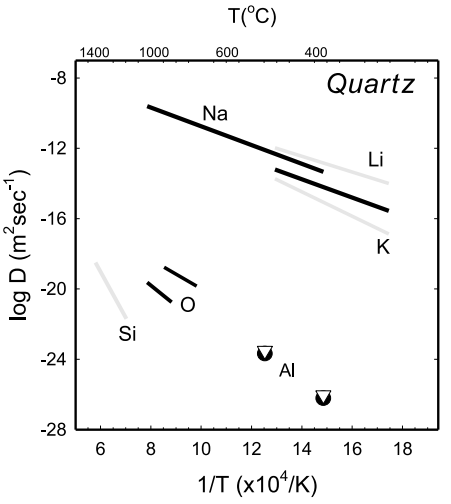

Fig. 10. Cation and oxygen diffusion in quartz. Sources for data: Na: [42,43]; Li, K: [42]; Al: [35]; O: [36–38]; Si: this study.

ences in activation enthalpies among individual materials are likely due to differences in the coupling of point defects that minimize the migration energy for Si through the lattice, and/or the characteristic 'extrinsicity' of the material (based on its impurity levels, non-stoichiometry, presence of aliovalent cations, and so on). In Fig. 12, we plot the compensation relation, using the data tabulated in [40], a few more recent results, and the findings from the present study. The compensation line can be described by the equation $E = 652.2 + 30.6 \times \log D_o$. Both the natural quartz and feldspars fall closely along the compensation trend. The fact that the feldspars do is interesting in light of the speculation of Béjina and Jaoul [40] that there is this commonality because all of the silicates contain the SiO_4 tetrahedron as a fundamental structural component, since the feldspars contain tetrahedra with Al as well. Béjina and Jaoul [40] note that their data were obtained for OH- and Al-free systems, but it appears that the presence of Al, even in the large concentrations present in aluminosilicate minerals, does not necessarily cause deviation from the compensation trend.

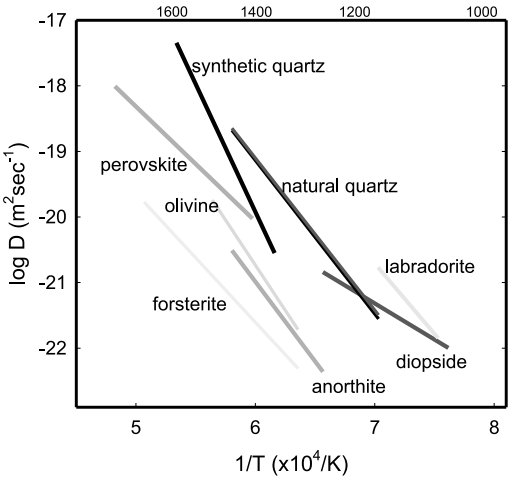

Fig. 11. Si diffusion in silicates. Sources for data: Mg–Fe olivine: [4]; forsterite: [39]; MgSi perovskite: [44]; diopside: [2]; synthetic quartz: [2]; labradorite, anorthite, natural quartz: this study.

8. Conclusions

Si diffusion in natural quartz and feldspar has been measured. The Arrhenius relation 6.40×10^{-6} exp $(-443 \pm 22$ kJ mol$^{-1}/RT)$ m^2 s^{-1} is obtained for Si diffusion in quartz parallel to c;

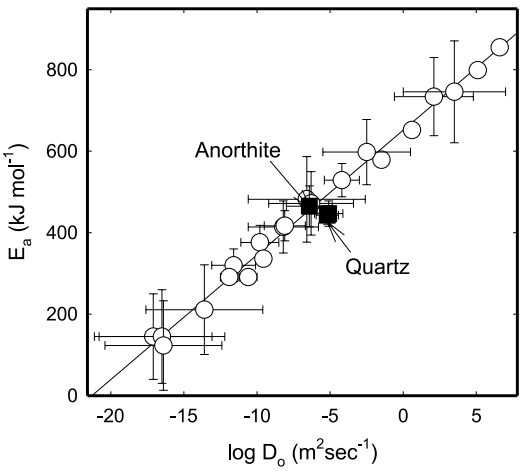

Fig. 12. Plot of activation energy (in kJ mol^{-1}) vs. the log of the pre-exponential factor D_o, showing that Si diffusion data for silicates conform well to the linear 'diffusion compensation' relation. The compensation line can be described by the equation $E = 652.2 + 30.6 \times \log D_o$. Data plotted are from [40], and sources cited for Fig. 11. Results from the present study (dark squares) are also plotted, and fall closely along the diffusion compensation trend.

little anisotropy for Si diffusion is evident. These diffusivities are consistent with findings of [2] for Si diffusivities in synthetic quartz obtained for diffusion anneals in air.

For anorthite, we obtain the Arrhenius relation 3.79×10^{-7} exp $(-465\pm50$ kJ mol$^{-1}/RT)$ m^2 s^{-1}. Si diffusion in more sodic plagioclase (oligoclase and labradorite) is faster than diffusion in anorthite, a finding consistent with that observed for other cations in feldspars. The results for anorthite and labradorite bracket the determination of CaAl–NaSi interdiffusion in bytownite under dry conditions by Grove et al. [1], suggesting that the rate-limiting process in CaAl–NaSi interdiffusion is Si diffusion.

In both quartz and feldspar, Si diffusion is the slowest of all cations measured, a finding not surprising given the +4 valence of Si and large site energies for tetrahedral sites in feldspars and Si sites in quartz. Si diffusion parameters obtained in the present study also conform well to the linear diffusion compensation trend for Si diffusivities in silicate minerals, in agreement with earlier observations in [40].

Acknowledgements

I thank Bruce Watson for helpful advice and discussion during the course of this work, and appreciate Bill Minarik's assistance with the experiments run under buffered conditions. I am also grateful to the National Museum of Natural History, Don Baker, and Don Miller for the feldspar samples. Insightful review comments by John Farver and Olivier Jaoul helped in improving the final manuscript. This work was supported by Grant EAR-9315051 from the National Science Foundation.*[KF]*

References

[1] T.L. Grove, M.B. Baker, R.J. Kinzler, Coupled CaAl-NaSi diffusion in plagioclase feldspar; experiments and applications to cooling rate speedometry, Geochim. Cosmochim. Acta 48 (1984) 2113–2121.
[2] F. Béjina, O. Jaoul, Silicon self-diffusion in quartz and diopside measured by nuclear micro-analysis methods, Phys. Earth Planet. Inter. 97 (1996) 145–162.
[3] B. Houlier, O. Jaoul, F. Abel, R.C. Liebermann, Oxygen and silicon self-diffusion in natural olivine at T = 1300 degrees C, Phys. Earth Planet. Inter. 50 (1988) 240–250.
[4] B. Houlier, M. Cheraghmakani, O. Jaoul, Silicon diffusion in San Carlos olivine, Phys. Earth Planet. Inter. 62 (1990) 329–340.
[5] J.V. Smith, W.L. Brown, Feldspar Minerals; Vol. 1, Crystal Structures, Physical, Chemical, and Microtextural Properties, 2nd edn., Springer-Verlag, Berlin, 1988, 828 pp.
[6] C.M. Graham, S.C. Elphick, A re-examination of the role of hydrogen in Al-Si interdiffusion in feldspars, Contrib. Mineral. Petrol. 104 (1990) 481–491.
[7] D.J. Cherniak, E.B. Watson, A study of strontium diffusion in K-feldspar, Na–K feldspar and anorthite using Rutherford backscattering spectroscopy, Earth Planet. Sci. Lett. 113 (1992) 411–425.
[8] D.J. Cherniak, Diffusion of Pb in plagioclase and K-feldspar measured by Rutherford backscattering spectroscopy and resonant nuclear reaction analysis, Contrib. Mineral. Petrol. 120 (1995) 358–371.
[9] R.A. Yund, Interdiffusion of NaSi-CaAl in peristerite, Phys. Chem. Miner. 13 (1986) 11–16.
[10] R.A. Yund, E. Snow, Effects of hydrogen fugacity and confining pressure on the interdiffusion rate of NaSi-CaAl in plagioclase, J. Geophys. Res. B 94 (1989) 10,662–10,668.
[11] M. Liu, R.A. Yund, NaSi-CaAl interdiffusion in plagioclase, Am. Mineral. 77 (1992) 275–283.
[12] R.A. Yund, J. Tullis, The effect of water, pressure, and strain on Al/Si order-disorder kinetics in feldspar, Contrib. Mineral. Petrol. 72 (1980) 297–302.
[13] J.R. Goldsmith, M. Jenkins, The high-low albite relations revealed by reversal of degree of order at high pressures, Am. Mineral. 70 (1985) 911–923.
[14] J.R. Goldsmith, The role of hydrogen in promoting Al–Si interdiffusion in albite ($NaAlSi_3O_8$) at high pressures, Earth Planet. Sci. Lett. 80 (1986) 135–138.
[15] J.R. Goldsmith, Al/Si interdiffusion in albite; effect of pressure and the role of hydrogen, Contrib. Mineral. Petrol. 95 (1987) 311–321.
[16] H. Kroll, R. Knitter, Al, Si exchange kinetics in sanidine and anorthoclase and modeling of rock cooling paths, Am. Mineral. 76 (1991) 928–941.
[17] D.J. Cherniak, E.B. Watson, A study of strontium diffusion in plagioclase using Rutherford backscattering spectroscopy, Geochim. Cosmochim. Acta 58 (1994) 5179–5190.
[18] D.J. Cherniak, REE diffusion in feldspar, Chem. Geol. 193 (2003) 25–41.
[19] D.J. Cherniak, Ba diffusion in feldspar, Geochim. Cosmochim. Acta 66 (2002) 1641–1650.
[20] K.P.R. Reddy, A.R. Cooper, Oxygen diffusion in sapphire, J. Am. Ceram. Soc. 65 (1982) 634–638.
[21] J. Hirvonen, A. Anttila, Self-diffusion in silicon as probed

by the (p,γ) resonance broadening method, Appl. Phys. Lett. 35 (1979) 703–705.
[22] D.S. Tannhauser, Concerning a systematic error in measuring diffusion constants, J. Appl. Phys. 27 (1956) 662.
[23] D.J. Cherniak, J.M. Hanchar, E.B. Watson, Rare earth diffusion in zircon, Chem. Geol. 134 (1997) 289–301.
[24] H.S. Carslaw, J.C. Jaeger, Conduction of Heat in Solids, 2nd edn., Clarendon, Oxford, 1986, 510 pp.
[25] B.J. Giletti, R.A. Yund, M. Semet, Silicon diffusion in quartz, Abstracts with Programs, Geol. Soc. Am. 8 (1976) 883–884.
[26] E.B. Watson, D.J. Cherniak, Lattice diffusion of Ar in quartz, with constraints on Ar solubility and evidence of nanopores, Geochim. Cosmochim. Acta 67 (2003) 2043–2062.
[27] R.D. Aines, G.R. Rossman, Water in minerals? A peak in the infrared, J. Geophys. Res. 89 (1984) 4059–4071.
[28] R.D. Aines, G.R. Rossman, The high-temperature behavior of trace hydrous components in silicate minerals, Am. Mineral. 70 (1984) 1169–1179.
[29] G. Baschek, W. Joahnnes, The estimation of NaSi-CaAl interdiffusion rates in peristerite by homogenization experiments, Eur. J. Mineral. 7 (1995) 295–307.
[30] B.J. Giletti, J.E.D. Casserly, Strontium diffusion kinetics in plagioclase feldspars, Geochim. Cosmochim. Acta 58 (1994) 3785–3793.
[31] B.J. Giletti, T.M. Shanahan, Alkali diffusion in plagioclase feldspar, Chem. Geol. 139 (1997) 3–20.
[32] T. LaTourette, G.J. Wasserburg, Mg diffusion in anorthite: implications for the formation of early solar system planetesimals, Earth Planet. Sci. Lett. 158 (1998) 91–108.
[33] H. Behrens, W. Johannes, H. Schmalzried, On the mechanisms of cation diffusion processes in ternary feldspars, Phys. Chem. Miner. 17 (1990) 62–78.
[34] J.R. Smyth, D.L. Bish, Crystal Structures and Cation Sites of the Rock-Forming Minerals, Allen and Unwin, Boston, MA, 1988.
[35] R. Pankrath, O.W. Flörke, Kinetics of Al-Si exchange in low and high quartz: calculation of Al diffusion coefficients, Eur. J. Mineral. 6 (1994) 435–457.
[36] P.F. Dennis, Oxygen self-diffusion in quartz under hydrothermal conditions, J. Geophys. Res. B 89 (1984) 4047–4057.
[37] P.F. Dennis, Oxygen self diffusion in quartz. Sixth progress report of research supported by N.E.R.C., 1981–1984, Prog. Exp. Petrol. 6 (1984) 260–265.
[38] Z.D. Sharp, B.J. Giletti, H.S. Yoder Jr., Oxygen diffusion rates in quartz exchanged with CO_2, Earth Planet. Sci. Lett. 107 (1991) 339–348.
[39] O. Jaoul, M. Poumellec, C. Froidevaux, A. Havette, Silicon diffusion in forsterite; a new constraint for understanding mantle deformation, in: F.D. Stacey, M.S. Paterson, A. Nicholas (Eds.), Anelasticity in the Earth, American Geophysical Union, Washington, DC, 1981.
[40] F. Béjina, O. Jaoul, Silicon diffusion in silicate minerals, Earth Planet. Sci. Lett. 153 (1997) 229–238.
[41] C. Zener, Theory of diffusion, in: W. Shockley, J.H. Hollomon, R. Maurer, F. Seitz (Eds.), Imperfections in Nearly Perfect Crystals, Wiley, New York, 1952, pp. 289–314.
[42] J. Verhoogen, Ionic diffusion and electrical conductivity in quartz, Am. Mineral. 37 (1952) 637–655.
[43] G.H. Frischat, Sodium diffusion in natural quartz crystals, J. Am. Ceram. Soc. 53 (1970) 357.
[44] D. Yamazaki, T. Kato, H. Yurimoto, E. Ohtani, M. Toriumi, Silicon self-diffusion in $MgSiO_3$ perovskite at 25 GPa, Phys. Earth Planet. Inter. 119 (2000) 299–309.